Osteoporos Int (2009) 20:123–132
DOI 10.1007/s00198-008-0632-0

ORIGINAL ARTICLE

Shortcomings of DXA to assess changes in bone tissue density and microstructure induced by metabolic bone diseases in rat models

A. Nazarian · E. Cory · R. Müller · B. D. Snyder

Received: 13 October 2007 / Accepted: 21 March 2008 / Published online: 31 May 2008

Abstract
Summary The aim of this study is to demonstrate the deficiencies of dual-energy X-ray absorptiometry (DXA), compared with quantitative computed tomography, to reflect and differentiate between changes in bone mineral density and microstructure that contribute to a well-defined finding of altered skeletal state for both osteoporosis and renal osteodystrophy induced by chronic renal insufficiency.
Introduction The aim of this study is to demonstrate the deficiencies of dual-energy X-ray absorptiometry (DXA), compared with quantitative CT, to reflect and differentiate between changes in bone mineral density and microstructure that contribute to a well-defined finding of altered skeletal state for both osteoporosis and renal osteodystrophy induced by chronic renal insufficiency.
Methods Forty-five female Sprague–Dawley rats were divided into three equal groups: control, ovariectomy, and nephrectomy. Following euthanasia, femurs were excised, divided into diaphyseal and distal metaphyseal sections, and subjected to DXA and micro-CT imaging and mechanical testing.
Results Ovariectomy does not affect the structural and mechanical properties of cortical bone material, but partial nephrectomy does adversely affect these properties. Both are verified by DXA and micro-CT imaging and mechanical testing. Meanwhile, nephrectomy does not affect trabecular bone microstructure or equivalent density, yet ovariectomy affects the trabecular microstructure. DXA is unable to detect changes in trabecular bone microstructure in relation to changes in their mechanical properties.
Discussion Dual energy X-ray absorptiometry measures the average bone mineral content in a 2D projected area and cannot differentiate whether the changes occur in the bone microstructure or equivalent bone tissue density. In contrast, micro-CT provides an accurate measurement of the changes in both equivalent bone tissue mineral density and microstructure for cancellous and cortical bone.

Keywords Animal model · Bone density · Bone tissue properties · DXA · Micro-CT · Microstructure · Osteomalacia · Osteopenia · Osteoporosis · Renal osteodystrophy

A. Nazarian and E. Cory have contributed equally to this work.

A. Nazarian · E. Cory · B. D. Snyder (✉)
Orthopedic Biomechanics Laboratory (OBL),
Beth Israel Deaconess Medical Center and Harvard Medical School,
330 Brookline Avenue, RN115,
Boston, MA 02215, USA
e-mail: bsnyder@bidmc.harvard.edu

B. D. Snyder
Department of Orthopaedic Surgery,
Children's Hospital, Harvard Medical School,
Boston, MA 02215, USA

A. Nazarian
Institute for Biomedical Engineering, University and ETH Zürich,
8044 Zürich, Switzerland

R. Müller
Institute for Biomechanics, ETH Zürich,
8093 Zürich, Switzerland

Introduction

Fragility fractures of the hip, spine or wrist are common causes of disability affecting 1.5 million Americans annually [1, 2]. A 50-year-old white woman has a 15–20% lifetime risk of sustaining a hip fracture associated with long-term morbidity and a 20–33% mortality rate 1 year after fracture [3]. Fragility fractures are caused by low bone mass and micro-architectural deterioration of

bone tissue [4]. The World Health Organization (WHO) has identified individuals at risk of fragility fractures based on their bone mineral density (BMD). BMD is measured by dual energy X-ray absorptiometry (DXA) at the hip, lumbar spine, wrist or calcaneus relative to that of a normal young adult. However, such fracture predictions based on BMD have been shown to be neither sensitive nor specific [5–9].

Fracture occurs when the applied load exceeds the load-bearing capacity of bone, as determined by its material and structural properties [10]. Bone strength depends on apparent bone density [11, 12] (ρ=bone mass/total specimen volume, $g.cm^{-3}$), which is the product of bone tissue density (ρ_{tiss} = bone mass/bone tissue volume, $g.cm^{-3}$) and bone volume fraction (BV/TV = bone tissue volume/total specimen volume, mm^3/mm^3). ρ_{tiss} reflects the organic matrix and the mineral composition of bone tissue, which contributes to its intrinsic material properties. BMD ($g.cm^{-2}$), on the other hand, is an areal projection of bone mineral density and *not* a true measure of bone density. BMD fails to distinguish changes in bone tissue composition from changes in bone tissue volume, an important distinction when diagnosing and treating diseases associated with low bone mass.

While osteoporosis (~ normal ρ_{tiss}, ↓↓ BV/TV) [13] is assumed to be the cause of most fragility fractures, 25-OH-vitamin D deficiency, a diagnosis not distinguished by DXA-assessed BMD, is observed in 50% of postmenopausal women in the population who fracture their hip (not including those residing in retirement homes) and in whom there is no other cause of low bone mass [14, 15]. Vitamin D deficiency can result in osteomalacia (↓↓ρ_{tiss}, ↓BV/TV), which has been diagnosed histologically (hypo-mineralized osteoid) in 13–33% of patients with hip fractures [16–20].

Therefore, DXA is unable to differentiate between metabolic bone diseases such as osteoporosis (OP) and renal osteodystrophy manifested as osteomalacia (OM), both of which cause *osteopenia* (altered skeletal state), but affect bone micro-structure and tissue mineralization differently at cortical and cancellous bone sites. In patients, *osteopenia* is diagnosed when BMD is >1 standard deviation (SD) below the mean for a young normal adult of the same sex, and *osteoporosis* is diagnosed when BMD is ≥2.5 SD below the mean for a young normal adult of the same sex [21].

Dual energy X-ray absorptiometry measurements are based on the aerial projection of a 3D construct, where trabecular and cortical bone components are integrated. In contrast, quantitative computed tomography, a 3D imaging modality, can provide information about specific changes in bone microstructure and tissue density for both cortical and cancellous bone. The ovariectomized (OVX) rat model has been widely used to study the effects of menopause on bone mass, trabecular microstructure, and fracture risk [22–30], and the partially nephrectomized (NFR) rat model has been used to study the effects of renal osteodystrophy manifested as osteomalacia on bone metabolism [31–37]. While the diagnostic guidelines of osteoporosis in an animal model have yet to be established, the term has been used interchangeably to refer to an altered skeletal state due to ovariectomy [38]. Therefore, we will use the established ovariectomy model as a surrogate for an osteoporosis animal model in conjunction with the nephrectomy-induced renal osteodystrophy model to demonstrate the deficiencies of DXA compared with quantitative computed tomography, and to reflect and differentiate between changes in bone mineral density and microstructure that contribute to a well-defined finding of altered skeletal state for both osteoporosis and renal osteodystrophy manifesting as osteomalacia. To that end, we hypothesize that DXA is unable to assess changes in bone tissue density and microstructure caused by metabolic bone diseases induced by ovariectomy and nephrectomy.

Materials and methods

Animal models

Thirty female Sprague–Dawley (SD, mass: 250–275 g, age: ~15 weeks) mature rats were obtained from Charles River Laboratories (Charles River, Charlestown, MA, USA) and were divided into three equally sized groups: the animals in the control group (CON) were not subject to any surgical or dietary interventions; the OVX group underwent ovariectomy (a week prior to the start of the study) to induce a state of low bone mass and micro-architectural deterioration [22–30] and the NFR group underwent five-sixth nephrectomy (a week prior to the start of the study) in addition to being placed on a modified diet containing 0.6% Ca and 1.2% P (from T0 until the end of the study) to induce renal osteodystrophy [31–37] (normal rodent diet contains 1.35% Ca and 1.04% P) and severe secondary hyperparathyroidism. Both surgical procedures were conducted at the animal supplier facility 1 week prior to the arrival of the animals at the laboratory (Fig. 1). The study protocol was approved by the Beth Israel Deaconess Medical Center's Institutional Animal Care and Use Committee (IACUC). Animals were weighed each week to assess changes in body mass over the study period.

Specimen geometry

A mid-diaphyseal (cortical bone only) and a distal metaphyseal (trabecular + cortical bone) segment was cut from each femur perpendicular to the anatomical axis between two parallel diamond wafering blades on a low-speed saw (Isomet, Buehler Corporation, Lake Bluff, IL, USA) under copious irrigation. The cortical midshaft segments (H: 5.99 mm ± 0.28 mm, ∅: 3.64 mm ± 0.24 mm) were cut to maintain a 2:1 height to diameter

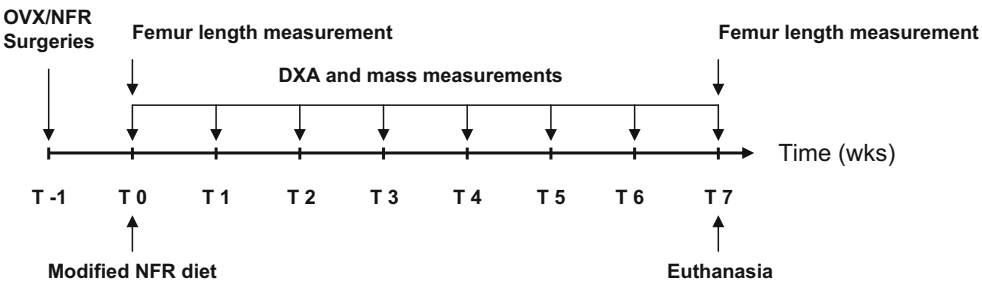

Fig. 1 Study timeline highlighting surgical interventions and measurements. DXA = dual energy X-ray absorptiometry; OVX = ovariectomized group; NFR = partially nephrectomized group

ratio [39], while the distal metaphyseal segments, with the thin cortex shaved off (H: 6.22 mm ± 0.73 mm, ∅: 4.84 mm ± 0.41 mm), were cut immediately above the growth plate, identified from anterior–posterior contact radiographs, to include the distal metaphyseal trabecular structure (Fig. 2). The metaphyseal cortex was shaved off under an established protocol at the laboratory using diamond wafering blades and visual magnification. The presence of cortical shell was ruled out via radiography during the process and subsequent micro-CT imaging. The cortical and trabecular segments underwent cleaning via sonic agitation (Fisher Scientific International, Hampton, NH, USA) while suspended in an equal mixture of water and ethyl alcohol for 20 min, followed by centrifugal removal of excess water and marrow at 9G for 15 min. The average mass and physical dimensions of each segment were measured (average of 3 measurements per case) using precision balance and calipers.

Imaging and image analysis

Bone mineral density (BMD) and bone mineral content (BMC) at the femoral diaphysis (cortical bone) and the distal femoral metaphysis (cancellous bone) were measured using DXA (Lunar PIXImus2; General Electric, Waukesha, WI, USA) on a weekly basis over a 7-week period. Two landmark-based analysis boxes, one to cover the cortical bone area and one to cover the distal femoral metaphysis, were used to assess BMD from DXA throughout the study. Additionally, femur lengths were measured using DXA images at the initial and final time points to assess animal growth over the course of the study. At the end of week 7, the animals were euthanized and both femurs were extracted. Sequential transaxial images through the entire femur were obtained using micro-computed tomography (micro-CT; Scanco Medical, Bassersdorf, Switzerland) at an isotropic voxel size of 20 μm, integration time of 250 ms, and beam energy and current of 70 keV and 0.114 mA respectively. Micro-CT imaging was performed on excised, cut (cortical), and cut and shaved off (trabecular) samples. A three-dimensional Gaussian filter (σ=0.8) with a limited, finite filter support [1] was used to suppress the noise in the volumes. The images were binarized to separate bone from background using an adaptive thresholding procedure. After thresholding, cortical bone volume fraction (Ct.BV/TV) and cortical thickness (Ct.Th) along with direct trabecular morphometric indices of bone volume fraction (BV/TV), bone surface density (BS/BV), structure model index (SMI), trabecular number (Tb.N), trabecular thickness (Tb.Th), trabecular thickness intra-individual standard deviation, calculated as the second moment of the Tb.Th histogram distribution (Tb.Th SD), trabecular spacing (Tb.Sp), trabecular spacing intra-individual standard deviation, calculated as the second moment of the Tb.Sp histogram distribution (Tb.Sp SD), degree of anisotropy (DA=length of the longest divided by the shortest MIL tensor), and connectivity density (Conn.D) were assessed for all images [40]. Additionally, equivalent bone mineral density ($\rho_m(I)$) was calculated using a hydroxyapatite phantom, supplied by the manufacturer, to convert X-ray

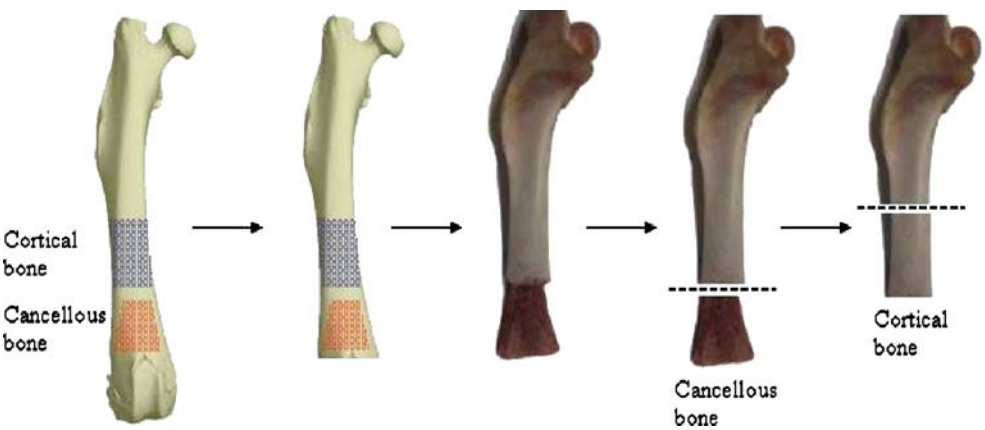

Fig. 2 An illustration of cortical and trabecular specimen preparation

attenuation coefficient (μ) to an equivalent density. This equivalent bone tissue mineral density (ρ_{equiv}, $g.cm^{-3}$) was calculated by summing $\Sigma[\rho_m(I)\cdot dv]$ over all voxels contained within the bone profiles visualized on each transaxial micro-CT image and dividing that sum by the total bone tissue volume, $BV = \Sigma\, dv_{bone}$. This method of bone mineralization measurement is prone to partial volume artifacts. However, this is a comparative study of samples with relatively similar size. So, the effects of partial volume artifacts can be considered uniform across the study; therefore, unlikely to affect the outcome of the study. The precision of dual energy absorptiometry to assess rat femoral BMD and BMC is less than 1.5% based on the existing system and the established protocol at our laboratory. Likewise, the precision of micro-computed tomographic assessment of 3D microstructural indices of excised rat bone samples is less than 0.5%.

Mechanical testing

At the conclusion of the study, all cortical and cancellous segments underwent compressive mechanical testing (Synergy 200; MTS, Prairie View, MN, USA). Specimens were preconditioned, using a triangular waveform, to 0.33% strain for seven cycles at a strain rate of 0.005 s^{-1}, followed by uniaxial compression to failure at a rate of 0.01 s^{-1}. Stiffness (K, $kN.mm^{-1}$) and yield load (L_{yield}, kN), representing extrinsic structural properties, were reported for the study. Stiffness was assessed by measuring the slope of the elastic region of the load displacement curve for the cortical and cancellous segments, and yield load was assessed as the point where the load–displacement curve ceased to be linear. Specimens were thawed out to room temperature and hydrated prior to mechanical testing and were stored in saline-soaked gauze at −20°C for the duration of the study.

Statistical analysis

Continuous data were assessed for normality using the Kolmogorov–Smirnov test. A power analysis indicated that 10 animals per group provided ±20% precision to measure the correlation between bone tissue and structural properties and measurements of bone strength with a 95% confidence interval around a moderate Pearson coefficient of 0.60 (nQuery Advisor, version 6.0; Statistical Solutions, Saugus, MA, USA). One-way analysis of variance (ANOVA) was conducted with animal model (CON, OVX, and NFR) as the independent variable, and BMD, BMC, mass, trabecular and cortical bone microstructural indices, ρ_{equiv} measured by micro-CT, and extrinsic mechanical properties as dependent variables. A repeated measure ANOVA test was conducted with animal model as the independent variable and BMC, BMD, body mass, and femur length over time as dependent variables. The SPSS statistical package (version 15.0; Chicago, IL, USA) was used for data analysis. All reported p values are two-tailed, with $p<0.05$ considered statistically significant.

Results

The normalized body mass (the mass at time 0) increased by 10.7%, 22.2%, and 28.7% for the rats in the CON, OVX, and NFR disease groups respectively from week 1 to week 7. Repeated measures ANOVA revealed that the normalized mass in the OVX and NFR groups was different from that of the CON group, yet no difference was observed between the two (OVX and NFR vs CON, $p<0.001$; OVX vs NFR, $p=0.31$; Fig. 3a). Average femur lengths between the CON, OVX, and NFR groups exhibited a nonsignificant increasing trend (3.3%, 1.9%, and 3.3%) over time from week 1 to 7 ($p>0.05$ for all cases). This trend was due to animal growth over the study period.

At week 7, the mid-diaphyseal (cortical) BMC of the CON group was not different from that of the OVX group ($p>0.99$), yet it was 14.8% more than that of the NFR group ($p<0.001$). Similarly, the mid-diaphyseal BMD of the CON group was not different from that of the OVX ($p=0.10$), yet was 16.0% more than that of the NFR ($p<0.001$). The metaphyseal (trabecular) BMC of the CON group was 7.6% and 16.5% more than those of the OVX ($p=0.04$) and NFR groups respectively ($p<0.001$). Also, the metaphyseal BMD of the CON group was 12.5% and 25.0% greater than those of the OVX ($p<0.001$) and NFR ($p<0.001$) groups. Over the course of the study, diaphyseal BMC and BMD measurements across all groups demonstrated an upward trend, with a downward slope for the NFR group from week 6 onward (Fig. 3b). Conversely, metaphyseal BMC and BMD maintained an increasing trend in the CON group throughout the study, while the OVX and NFR groups exhibited a downward slope up to weeks 3 and 4, followed by an increasing slope from then onward (Fig. 3c, Table 1).

Micro-CT assessment showed that mid-diaphyseal equivalent bone tissue density of the CON group was not different from that of the OVX group ($p=0.07$), yet it was 19.0% greater than the NFR group ($p=0.001$). Cortical BV/TV of the CON group was not different from that of the OVX group ($p=0.23$); however, it was 16.4% greater than that of the NFR group ($p=0.01$). Additionally, the cortical thicknesses of the CON and the OVX group were not different ($p=0.59$); however, the cortical thickness of the NFR group was half that of the CON group ($p=0.001$; Table 2).

Micro-CT assessment showed that the distal metaphyseal-equivalent bone tissue density of the CON group was not different from those of the OVX ($p=0.16$) and NFR

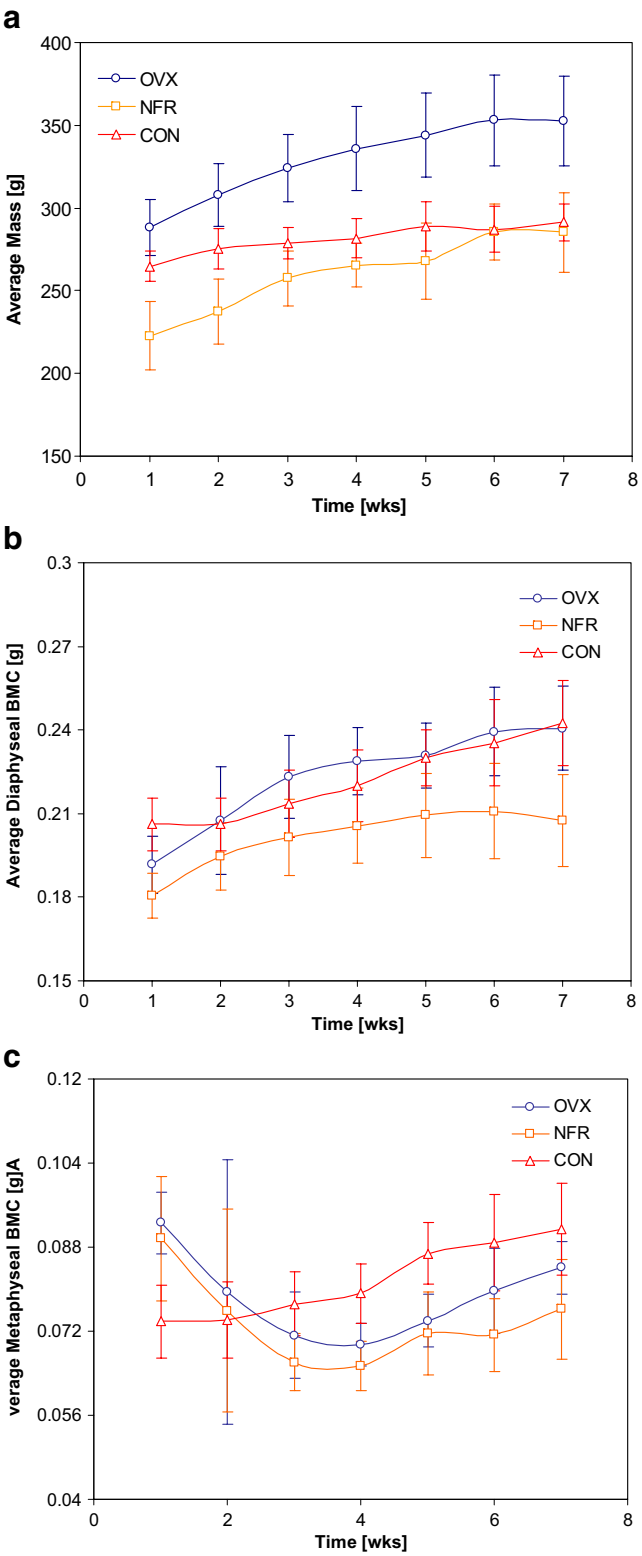

Fig. 3 **a** Average mass of the animals in each group over the study period. **b** Average mid-diaphyseal bone mineral content (BMC) of the animals in each group over the study period. **c** Average distal metaphyseal BMC of the animals in each group over the study period. CON = control group; OVX = ovariectomized group; NFR = partially nephrectomized group

Table 1 Dual energy absorptiometry (DXA)-generated bone mineral content (BMC) and bone mineral density (BMD) values for the mid-diaphyseal and distal metaphyseal regions

Group	Mid-diaphyseal		Distal metaphyseal	
	BMC (g)	BMD (g.cm^{-2})	BMC (g)	BMD (g.cm^{-2})
CON	0.243 (0.015)	0.243 (0.011)	0.091 (0.008)	0.232 (0.018)
OVX	0.240 (0.015)	0.232 (0.012)	0.084 (0.005)	0.203 (0.015)
NFR	0.207 (0.016)	0.204 (0.015)	0.076 (0.009)	0.174 (0.018)

CON = control group; OVX = ovariectomized group; NFR = partially nephrectomized group

(p=0.10) groups. The trabecular BV/TV of the CON group was 55% greater than that of the OVX group (p<0.003) and was not different from that of the NFR group (p=0.90). Corresponding changes were also noted in the trabecular microstructure: the Tb.N of the CON group was 52% greater than that of the OVX group (p=0.001), yet not different from that of the NFR group (p=0.99); the Tb.Sp of the CON group was 150% less than that of the OVX group (p<0.001) and was not different from that of the NFR group (p=0.44). The intra-individual standard deviation of OVX trabecular spacing was 277 times greater than that of the CON group (p<0.001); however, no difference was observed between the CON and NFR groups (p=0.07). The Tb.Th of the OVX and NFR groups was 21% and 16% less than that of the CON group (p<0.001 for both cases) respectively. Likewise, the intra-individual standard deviation of the trabecular thickness of the OVX and NFR groups was 48% and 51% greater than that of the CON group (p<0.001 for both cases).

The specific bone surface (BS/BV) of the OVX group was 34% greater than that of the CON group (p=0.001); however, no difference was observed between the CON and NFR groups (p=0.27). Trabecular connectivity density (Conn.D) of the CON group was 55% greater than that of the OVX group (p=0.006), but 46% less than that of the NFR group (p=0.008). The structure model index (SMI) of the OVX group was 104% greater (more rod-like) than that of the CON group (p=0.010), while no significant difference was observed between the SMI values of the CON and NFR groups (p=0.17). The SMI scale ranges from 1 to 3, where 1

Table 2 Micro-computed tomography (micro-CT)-generated equivalent density and structural indices for the mid-diaphyseal region

Group	ρ_{equiv} (g.cm^{-3})	BV/TV (mm^3/mm^3)	Ct.Th (mm)
CON	1.169 (0.018)	0.587 (0.028)	0.522 (0.026)
OVX	1.228 (0.013)	0.621 (0.044)	0.565 (0.036)
NFR	0.946 (0.015)	0.492 (0.083)	0.259 (0.172)

CON = control group; OVX = ovariectomized group; NFR = partially nephrectomized group; ρ_{equiv} = equivalent bone density; BV/TV = bone volume fraction; Ct.Th = cortical thickness

Table 3 Micro-CT-generated equivalent density and microstructural indices for the distal metaphyseal region

Group	ρ_{equiv} (g.cm^{-3})	BS/BV (mm^2/mm^3)	BV/TV (mm^3/mm^3)	Tb.N (1/mm)	Tb.Sp (mm)	Tb.Sp SD	Tb.Th (mm)	Tb.Th SD	Conn.D (1/mm^3)	DA (–)	SMI (–)
CON	0.763 (0.065)	14.436 (2.905)	0.478 (0.067)	4.884 (0.345)	0.191 (0.019)	0.081 (0.017)	0.154 (0.028)	0.070 (0.026)	59.967 (11.795)	1.355 (0.139)	0.876 (0.303)
OVX	0.748 (0.058)	19.378 (1.545)	0.215 (0.074)	2.331 (0.579)	0.477 (0.095)	0.308 (0.087)	0.122 (0.007)	0.037 (0.009)	26.824 (13.122)	0.665 (0.187)	1.773 (0.363)
NFR	0.758 (0.055)	16.074 (3.068)	0.456 (0.100)	4.649 (0.718)	0.267 (0.018)	0.161 (0.155)	0.129 (0.019)	0.034 (0.006)	87.806 (19.023)	0.336 (0.117)	0.785 (0.585)

CON = control group; OVX = ovariectomized group; NFR = partially nephrectomized group; ρ_{equiv} = equivalent bone density; BS/BV = bone surface density; BV/TV = bone volume fraction; Tb.N = trabecular number; Tb.Sp = trabecular spacing; Tb.Sp SD = standard deviation of trabecular spacing; Tb.Th = trabecular thickness; Tb.Th SD = standard deviation of trabecular thickness; Conn.D = connectivity density; DA = degree of anisotropy; SMI = structure model index

Table 4 Extrinsic mechanical properties of the mid-diaphyseal and distal metaphyseal regions

Group	Mid-diaphyseal		Distal metaphyseal	
	K (kN/mm)	L_{ULT} (kN)	K (kN/mm)	L_{ULT} (kN)
CON	5.90 (1.36)	0.63 (0.14)	1.46 (0.33)	0.15 (0.02)
OVX	5.99 (1.47)	0.60 (0.21)	0.86 (0.35)	0.12 (0.02)
NFR	2.25 (0.83)	0.29 (0.17)	1.90 (0.46)	0.19 (0.03)

CON = control group; OVX = ovariectomized group; NFR = partially nephrectomized group; K = stiffness; L_{ULT} = ultimate load

refers to a predominantly plate-like structure, and 3 refers to a predominantly cylindrical structure. The degree of trabecular anisotropy (DA) was 51% and 75% lower in the OVX and NFR groups respectively, in comparison to the CON group ($p<0.001$ for both cases; (DA=1 isotropic and DA>1 anisotropic; Table 3).

Mid-diaphyseal (cortical) stiffness of the CON group was not different from that of the OVX group ($p= 0.23$), yet it was 62% greater than that of the NFR group ($p=0.02$). Similarly, the yield load of the CON group was not different from that of the OVX group ($p=0.34$), but was 55% greater than that of the NFR group ($p=0.80$). Distal metaphyseal stiffness of the CON group was 41% greater than that of the OVX group ($p=0.01$), but was 30% smaller than that of the NFR group ($p=0.02$). Finally, the yield load of the CON group was 23% greater than that of the OVX group ($p=0.01$) and 23% smaller than that of the NFR group ($p=0.01$; Table 4).

Discussion

Dual energy X-ray absorptiometry imaging reported non-significant decreasing trends in cortical BMC and its derivative BMD in ovariectomized animals, while micro-

Fig. 4 **a** Percentage changes in the density and in the structural and mechanical properties of the mid-diaphyseal ovarietcomized group (OVX) and the partially nephrectomized group (NFR) compared with the control group (CON). **b** Representative micro-CT cross-sections from the mid-diaphysis illustrate cortical bone density and morphology for the CON, OVX, and NFR groups. Cross-sections from the distal metaphysis illustrate trabecular bone morphology for the CON, OVX, and NFR groups. More significant cortical changes are observed in the NFR specimen, yet more significant trabecular changes are observed in the OVX specimen. **c** Percentage changes in the density and microstructural and mechanical properties of distal metaphyseal OVX and NFR compared with CON. *Asterisk* denotes significance ($p<0.05$). BMC = bone mineral content; BMD = bone mineral density; ρ_{equiv} = equivalent bone density; BV/TV = bone volume fraction; Ct.Th = cortical thickness; K = stiffness; L_{yield} = yield load; Tb.N = trabecular number; Tb.Th = trabecular thickness; Tb.Sp = trabecular spacing; Conn.D = connectivity density; SMI = structure model index; DA = degree of anisotropy; BS/BV = bone surface density; Th SD = standard deviation of the trabecular thickness; Sp SD = standard deviation of trabecular spacing

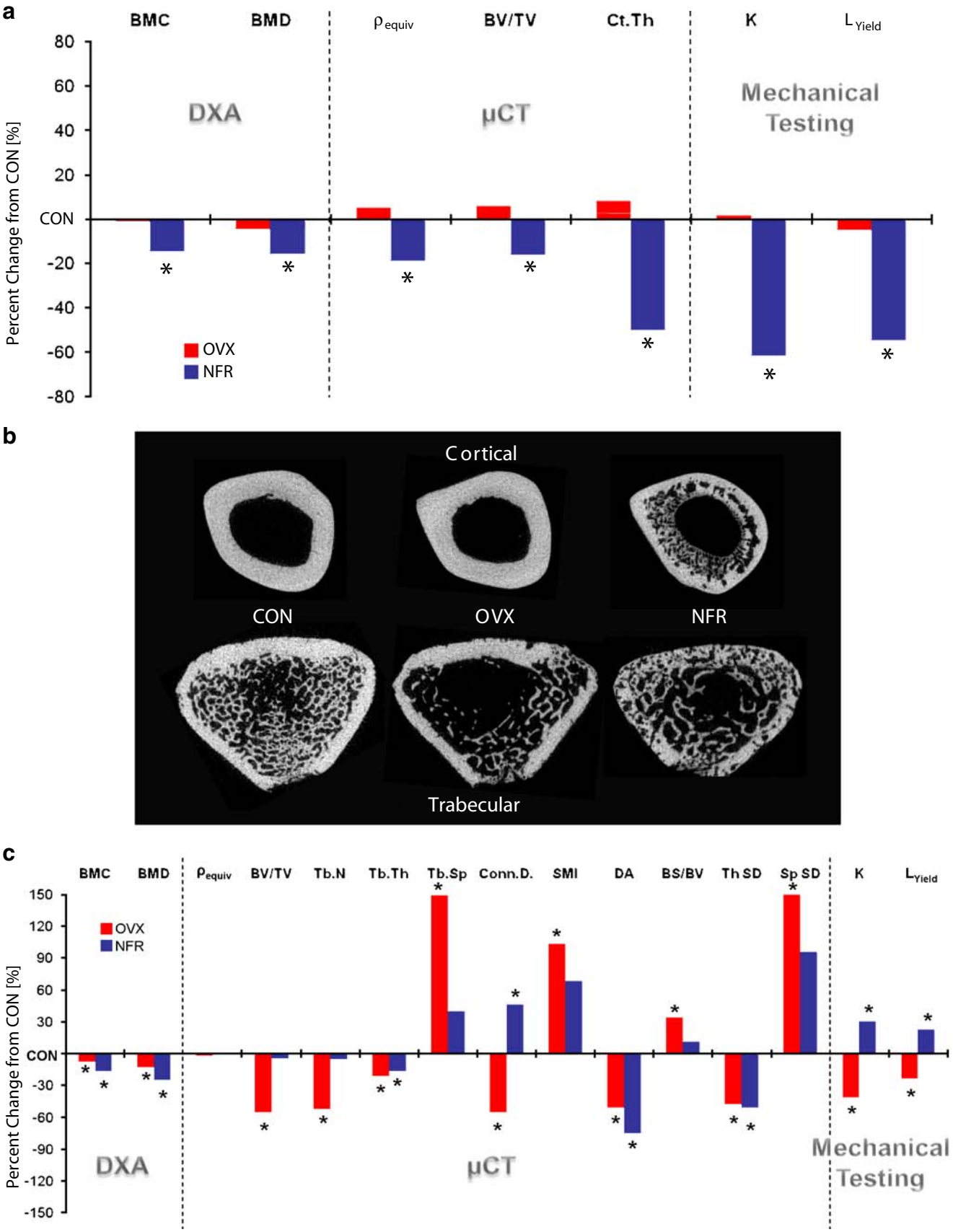
a
BMC
BMD
ρ equiv
BV/TV
Ct.Th
K
L Yield
DXA
μCT
Mechanical Testing
Percent Change from CON [%]
80
60
40
20
CON
-20
-40
-60
-80
OVX
NFR
b
Cortical
CON
OVX
NFR
Trabecular
c
BMC
BMD
ρequiv
BV/TV
Tb.N
Tb.Th
Tb.Sp
Conn.D.
SMI
DA
BS/BV
Th SD
Sp SD
K
LYield
OVX
NFR
Percent Change from CON [%]
150
120
90
60
30
CON
-30
-60
-90
-120
-150
DXA
μCT
Mechanical Testing

CT imaging revealed small and nonsignificant increasing trends in cortical equivalent tissue density, bone volume fraction, and cortical thickness. In the meantime, compressive mechanical testing of OVX samples showed a nonsignificant increasing trend in stiffness and a decreasing one in yield load. Therefore, it is reasonable to assume that ovariectomy results in no changes in the material, structural, and mechanical properties of femoral cortical bone after 7 weeks, as shown by DXA and micro-CT imaging (Fig. 4a). The increasing trend observed in micro-CT-generated tissue density, bone volume fraction, and cortical thickness could be interpreted as a small compensatory effect in countering the adverse changes in trabecular bone structure and mechanics due to ovariectomy.

Dual energy X-ray absorptiometry imaging reported a significant reduction (~15%) in cortical BMC and BMD values in partially nephrectomized animals, while micro-CT imaging reported a significant reduction in cortical equivalent bone tissue density (~19%), bone volume fraction (~16%), and cortical thickness (~50%). In the mean time, compressive mechanical testing of partially nephrectomized specimens reported at least a 55% reduction in cortical stiffness and yield load. While cortical tissue density and volume fraction were adversely affected by partial nephrectomy; it was the significant decrease in cortical thickness that corresponded to the loss of compressive mechanical properties at the scale observed, a process not detected by DXA imaging. Decreases in cortical thickness are primarily due to resorption along the endosteal surface of the diaphysis (Fig. 4b) as also reported by other researchers [33].

Dual energy X-ray absorptiometry imaging reported significant reductions in distal metaphyseal BMC and BMD in ovariectomized and partially nephrectomized animals. However, mechanical testing results indicated a significant loss of stiffness and yield load in ovariectomized bones, and gain of stiffness and yield load in the case of the partially nephrectomized bones (Fig. 4c). The inconsistency of the DXA results with respect to the mechanical data attest to the interplay of material and structural properties of bone with concomitant changes in bone biomechanics responding to different pathologic processes, and the inability of DXA to distinguish these cases in animal models. Results from micro-CT imaging provide further insight into this phenomenon. Connectivity density is shown to be the only structural predictor of trabecular stiffness and yield load, as it predicts the respective decrease and increase in trabecular mechanical properties of ovariectomized and partially nephrectomized animals. However, equivalent tissue density is shown to be unaffected by either process significantly over the course of the study. It is very likely that some changes in trabecular tissue level occur in the OVX and NFR animals, but these changes seem to have little influence on macro-scale mechanical properties, thereby emphasizing the superiority of structure over material in assessing the mechanical properties of bone.

In ovariectomized animals, loss of bone tissue volume in the form of thinning and disappearance of rod-like trabeculae and fenestration of plate-like elements with subsequent conversion to rod-like elements resulted in drops in bone volume fraction and in trabecular number and thickness, with concurrent increases in trabecular spacing and specific bone surface. This was further verified by increases in the SMI values, suggesting a more rod-like structure for the existing network. In partially nephrectomized animals, no changes were observed in the bone volume fraction, trabecular number, trabecular spacing, specific bone surface, and structure model index. But, trabecular thickness was adversely affected by partial nephrectomy. Therefore, partial nephrectomy has little effect on trabecular microstructure over an 8-week period.

The SMI, as derived by Hildebrand and Ruegsegger, is a three-dimensional method used to quantify the architectural type of cancellous bone based on the frequently used classifications of “rod-like” and “plate-like” structures. An ideal plate-like element has an SMI value of 0, whereas an ideal rod-like element has an SMI value of 3 [41]. Connectivity, on the other hand, is defined as a measure of the degree to which a structure is multiply connected, and hence, for a network, reports the maximal number of branches that can be broken before the structure is separated into two parts [42]. The increase in OVX SMI values in comparison to those in CON animals is resultant from the conversion of plate-like elements to rod-like elements. Fenestration of the plate-like elements is partially responsible for this conversion. However, no such conversion is observed in the NFR bones, as evidenced by the lack of change in their SMI values. On the other hand, the loss of trabecular network, as shown by decreases in bone volume fraction and trabecular number values, is reflected in the decreased connectivity density values of the animals in the OVX group. However, the trabecular thickness of the bones in the NFR group is smaller than those in the CON group, resulting in increased trabecular spacing. A portion of this trabecular resorption can result in the fenestration of some plate-like elements, which in the absence of a loss of rod-like trabeculae (as observed in OVX bones), can generate an artificial increase in the connectivity density values. This is further observed by an increase in the connectivity density values of the NFR bones.

The significant increase in the standard deviation of the intra-individual trabecular spacing of OVX reflects an increase in the heterogeneity of the microstructure and non-uniform removal of the trabeculae, resulting in reduced mechanical properties. This heterogeneity is not observed in the NFR bones, further confirmed by the absence of adverse effects on mechanical properties. The increase in

the standard deviations of intra-individual trabecular thickness of OVX and NFR do not appear to have any effects on their respective mechanical properties, nor do the decreased degrees of anisotropy in the two models.

Control animals demonstrated a slight trend of weight gain up to week 5, with an onward plateau thereafter; and the ovariectomized and partially nephrectomized groups maintained parallel and steady patterns of weight gain over the course of the study. The increased body mass in the OVX and NFR groups was due to ovariectomy and leucophlegmatia secondary to renal failure respectively.

A study by Jokihaara et al. using DXA imaging of whole left femurs reported a decrease in the total BMD of nephrectomized animals, whereas BMD values reached normal values (controls) in nephrectomized animals that were on an increased Ca diet (3%) [33]. They also reported decreased femoral midshaft BMD in nephrectomized animals and no changes in cross-sectional area and cortical thickness via quantitative computed tomographic imaging [33]. The discrepancy between cortical thickness values reported by Jokihaara et al. and this study may be explained by the increased resolution of micro-CT imaging. Microfocus CT imaging of nephrectomized rat trabecular bones reported slightly decreased BV/TV, BMD, Tb.N, Tb.Th, and connectivity density values in nephrectomized animals [35]. The discrepancy in the microstructure results between the two studies could be explained by two different imaging modalities used to obtain the microstructural indices. Laib et al. reported decreased BV/TV, Tb.N, Tb.th, and connectivity density in ovariectomized rats (110 days post-surgery). They also reported increases in SMI and Tb.Sp using a similar micro-CT imaging system [43].

Osteopenia [44–46] has been used interchangeably with osteoporosis [38] in animal studies, in reference to an ovariectomy-/orchiectomy-induced altered skeletal state. As there are no histologic- or guideline-based definitions associated with these terminologies for animal studies, their usage in the literature is uninformative and misleading.

Ovariectomy-induced changes in the skeletal state are caused primarily by changes in trabecular microstructure, reflecting its greater surface area and remodeling potential in comparison to cortical bone, further verified by no changes observed in equivalent bone tissue density of OVX trabecular bones. This is in contrast to renal osteodystrophy, where equivalent tissue density and structural level changes are observed in the cortical bones, but very little change observed in trabecular bone. It is quite possible that nephrectomy might alter the trabeculae in ways undetectable by μCT imaging. Therefore, further analysis using histomorphometry and/or synchrotron radiation could reveal such possible changes at a sub-micro level. DXA measures the average bone mineral content in a 2D projected area and cannot differentiate whether the changes occur in the bone microstructure or equivalent bone tissue density. In the meantime, DXA provides advantages such as low cost, low radiation dosage, and the ability to perform serial measurement in a relatively fast and simple manner. In contrast, micro-CT provides an accurate measurement of the changes in both equivalent bone tissue mineral density and microstructure in cancellous and cortical bone. This study was performed on animals using equipment designed for research use. It is plausible that these results could be duplicated in humans with equipment designed for clinical use. DXA systems used for clinical applications are designed based on the same principles as the DXA systems used in research. However, the modes of analysis are slightly different, partially due to the nature of the definition of osteoporosis by the WHO or lack thereof for research animals. On the other hand, with the recent development and marketing of Xtreme CT systems for clinical use by Scanco Medical AG, accurate assessment of 3D microstructural indices of bones in a clinical setting has become a reality. This suggests that in a clinical setting, DXA can be used as a screening tool for a nonspecific altered skeletal state, but the specific diagnosis should be predicated on quantitative high resolution CT measurements of bone tissue density and microstructure.

Acknowledgements The authors would like to acknowledge the Komen Foundation for providing financial support for this project (BDS Grant No: BCTR0403271). Additionally, they would like to acknowledge the efforts of Michael Bohanske, John Muller, Laura Gould, and Jeffrey O'Connell from the Orthopedic Biomechanics Laboratory with specimen preparation and testing.

Conflicts of interest None.

References

1. Riggs BL, Melton LJ III (1995) The worldwide problem of osteoporosis: insights afforded by epidemiology. Bone 17:505S–511S
2. Chrischilles EA, Butler CD, Davis CS, Wallace RB (1991) A model of lifetime osteoporosis impact. Arch Intern Med 151:2026–2032
3. Roche JJ, Wenn RT, Sahota O, Moran CG (2005) Effect of comorbidities and postoperative complications on mortality after hip fracture in elderly people: prospective observational cohort study. BMJ 331:1374
4. Consensus Development Conference (1993) Diagnosis, prophylaxis, and treatment of osteoporosis. Am J Med 94:646–650
5. Schuit SC, van der Klift M, Weel AE et al (2004) Fracture incidence and association with bone mineral density in elderly men and women: the Rotterdam Study. Bone 34:195–202
6. Cummings SR, Karpf DB, Harris F et al (2002) Improvement in spine bone density and reduction in risk of vertebral fractures during treatment with antiresorptive drugs. Am J Med 112:281–289
7. Heaney RP (2003) Is the paradigm shifting? Bone 33:457–465

8. Bauer DC, Black DM, Garnero P et al (2004) Change in bone turnover and hip, non-spine, and vertebral fracture in alendronate-treated women: the Fracture Intervention Trial. J Bone Miner Res 19:1250–1258
9. Riggs BL, Melton LJ III (2002) Bone turnover matters: the raloxifene treatment paradox of dramatic decreases in vertebral fractures without commensurate increases in bone density. J Bone Miner Res 17:11–14
10. Hayes WC, Bouxsein ML (1997) Biomechanics of cortical and trabecular bone: implication for assessment of fracture risk. In: Mow VC, Hayes WC (eds) Basic orthopaedic biomechanics. Lippincott-Raven, Philadelphia, pp 69–112
11. Rice JC, Cowin SC, Bowman JA (1988) On the dependence of the elasticity and strength of cancellous bone on apparent density. J Biomech 21:155–168
12. Snyder SM, Schneider E (1991) Estimation of mechanical properties of cortical bone by computed tomography. J Orthop Res 9:422–431
13. Favus MJ (ed) (2006) Primer on the metabolic bone diseases and disorders of mineral metabolism. American Society for Bone and Mineral Research, Washington, DC
14. LeBoff MS, Kohlmeier L, Hurwitz S, Franklin J, Wright J, Glowacki J (1999) Occult vitamin D deficiency in postmenopausal US women with acute hip fracture. JAMA 281:1505–1511
15. Glowacki J, Hurwitz S, Thornhill TS, Kelly M, LeBoff MS (2003) Osteoporosis and vitamin-D deficiency among postmenopausal women with osteoarthritis undergoing total hip arthroplasty. J Bone Joint Surg Am 85-A:2371–2377
16. Aaron J, Gallagher JC, Nordin BE (1974) Osteomalacia [letter]. Lancet 1:939
17. Aaron J, Gallagher JC, Nordin BE (1974) Osteomalacia and femoral fractures [letter]. Lancet 1:572
18. Chalmers J, Barclay A, Davison AM, Macleod DA, Williams DA (1969) Quantitative measurements of osteoid in health and disease. Clin Orthop Relat Res 63:196–209
19. Sokoloff L (1978) Occult osteomalacia in American (U.S.A.) patients with fracture of the hip. Am J Surg Pathol 2:21–30
20. Lips P, Netelenbos JC, Jongen MJ et al (1982) Histomorphometric profile and vitamin D status in patients with femoral neck fracture. Metab Bone Dis Relat Res 4:85–93
21. Kanis JA, Melton LJ III, Christiansen C, Johnston CC, Khaltaev N (1994) The diagnosis of osteoporosis. J Bone Miner Res 9:1137–1141
22. Miller SC, Wronski TJ (1993) Long-term osteopenic changes in cancellous bone structure in ovariectomized rats. Anat Rec 236:433–441
23. Reddy Nagareddy P, Lakshmana M (2005) Assessment of experimental osteoporosis using CT-scanning, quantitative X-ray analysis and impact test in calcium deficient ovariectomized rats. J Pharmacol Toxicol Methods 52:350–355
24. Yao W, Hadi T, Jiang Y, Lotz J, Wronski TJ, Lane NE (2005) Basic fibroblast growth factor improves trabecular bone connectivity and bone strength in the lumbar vertebral body of osteopenic rats. Osteoporos Int 16:1939–1947
25. Ito M, Nishida A, Aoyagi K, Uetani M, Hayashi K, Kawase M (2005) Effects of risedronate on trabecular microstructure and biomechanical properties in ovariectomized rat tibia. Osteoporos Int 16:1042–1048
26. Hornby SB, Evans GP, Hornby SL, Pataki A, Glatt M, Green JR (2003) Long-term zoledronic acid treatment increases bone structure and mechanical strength of long bones of ovariectomized adult rats. Calcif Tissue Int 72:519–527
27. Ogawa K, Hori M, Takao R, Sakurada T (2005) Effects of combined elcatonin and alendronate treatment on the architecture and strength of bone in ovariectomized rats. J Bone Miner Metab 23:351–358
28. Kaczmarczyk-Sedlak I, Janiec W, Pytlik M et al (2005) Effect of administration of etidronate and retinol on bone mechanical properties in ovariectomized rats. Pharmacol Rep 57:203–211
29. Guo XE, Goldstein SA (2000) Vertebral trabecular bone microscopic tissue elastic modulus and hardness do not change in ovariectomized rats. J Orthop Res 18:333–336
30. Wang L, Orhii PB, Banu J, Kalu DN (2001) Effects of separate and combined therapy with growth hormone and parathyroid hormone on lumbar vertebral bone in aged ovariectomized osteopenic rats. Bone 28:202–207
31. Feng JQ, Ward LM, Liu S et al (2006) Loss of DMP1 causes rickets and osteomalacia and identifies a role for osteocytes in mineral metabolism. Nat Genet 38:1310–1315
32. Turner CH, Owan I, Brizendine EJ, Zhang W, Wilson ME, Dunipace AJ (1996) High fluoride intakes cause osteomalacia and diminished bone strength in rats with renal deficiency. Bone 19:595–601
33. Jokihaara J, Jarvinen TL, Jolma P et al (2006) Renal insufficiency-induced bone loss is associated with an increase in bone size and preservation of strength in rat proximal femur. Bone 39:353–360
34. Miller MA, Chin J, Miller SC, Fox J (1998) Disparate effects of mild, moderate, and severe secondary hyperparathyroidism on cancellous and cortical bone in rats with chronic renal insufficiency. Bone 23:257–266
35. Kazama JJ, Iwasaki Y, Yamato H et al (2003) Microfocus computed tomography analysis of early changes in bone microstructure in rats with chronic renal failure. Nephron 95:e152–e157
36. Brkovic D, Linke J, Jakse G, Bauss F (2005) Changes in bone structure after augmentation cystoplasty in chronic uraemic rats. BJU Int 95:1066–1070
37. Freesmeyer MG, Abendroth K, Faldum A, Krauss C, Stein G (2001) Comparison of peripheral bone and body axis skeleton in a rat model of mild-to-moderate renal failure in the presence of physiological serum levels of calcitropic hormones. Bone 29:258–264
38. Melhus G, Solberg LB, Dimmen S, Madsen JE, Nordsletten L, Reinholt FP (2007) Experimental osteoporosis induced by ovariectomy and vitamin D deficiency does not markedly affect fracture healing in rats. Acta Orthop 78:393–403
39. Keaveny TM, Borchers RE, Gibson LJ, Hayes WC (1993) Theoretical analysis of the experimental artifact in trabecular bone compressive modulus. J Biomech 26:599–607
40. Hildebrand T, Laib A, Muller R, Dequeker J, Ruegsegger P (1999) Direct three-dimensional morphometric analysis of human cancellous bone: microstructural data from spine, femur, iliac crest, and calcaneus. J Bone Miner Res 14:1167–1174
41. Hildebrand T, Ruegsegger P (1997) Quantification of bone microarchitecture with the structure model index. Comput Methods Biomech Biomed Eng 1:15–23
42. Odgaard A, Gundersen HJ (1993) Quantification of connectivity in cancellous bone, with special emphasis on 3-D reconstructions. Bone 14:173–182
43. Laib A, Kumer JL, Majumdar S, Lane NE (2001) The temporal changes of trabecular architecture in ovariectomized rats assessed by MicroCT. Osteoporos Int 12:936–941
44. Ocarino NM, Marubayashi U, Cardoso TG et al (2007) Physical activity in osteopenia treatment improved the mass of bones directly and indirectly submitted to mechanical impact. J Musculoskelet Neuronal Interact 7:84–93
45. Jiang SD, Shen C, Jiang LS, Dai LY (2007) Differences of bone mass and bone structure in osteopenic rat models caused by spinal cord injury and ovariectomy. Osteoporos Int 18:743–750
46. Iwaniec UT, Moore K, Rivera MF, Myers SE, Vanegas SM, Wronski TJ (2007) A comparative study of the bone-restorative efficacy of anabolic agents in aged ovariectomized rats. Osteoporos Int 18:351–362